Magnetic Structure of MnO at 10 K from Total Neutron Scattering Data

Andrew L. Goodwin,[1] Matthew G. Tucker,[1] Martin T. Dove,[1,*] and David A. Keen[2,3]

[1]*Department of Earth Sciences, Cambridge University, Downing Street, Cambridge CB2 3EQ, United Kingdom*
[2]*Department of Physics, Oxford University, Clarendon Laboratory, Parks Road, Oxford OX1 3PU, United Kingdom*
[3]*ISIS Facility, Rutherford Appleton Laboratory, Chilton, Didcot, Oxfordshire OX11 0QX, United Kingdom*

(Received 24 October 2005; published 2 February 2006)

Total neutron scattering data from a powdered sample of MnO collected at 10 K have been analyzed using the reverse Monte Carlo method to refine the nuclear and magnetic structure. The results give the first unambiguous assignment of the average magnetic structure. The magnetic moments are aligned ferromagnetically within (111) sheets with the magnetization vectors of alternate sheets along axes parallel and antiparallel to the $\langle 11\bar{2}\rangle$ directions, albeit with a small modulated out-of-plane component. Small displacements of Mn and O (modulated with the same periodicity) accompany the magnetic ordering and both atomic and magnetic structures may be described in the monoclinic space group $C2$.

DOI: 10.1103/PhysRevLett.96.047209 PACS numbers: 75.25.+z, 02.70.Uu, 61.12.Ex

The classical antiferromagnet MnO has been widely studied as a representative of the family of first-row transition-metal monoxides. These materials show a variety of unusual insulating and magnetic properties, and provide benchmarks with which to test and develop our understanding of magnetic phenomena at the atomic scale. It is somewhat alarming then to find that details of the ordered magnetic structure of MnO—including properties such as the axis of spin alignment—remain undetermined. At temperatures above its ordering (Néel) temperature T_N of 118 K, the MnO lattice has the cubic NaCl-type structure; the transition from this paramagnetic phase to an antiferromagnetic phase at T_N is accompanied by a cubic-to-rhombohedral lattice distortion and is driven by nearest-neighbor and next-nearest-neighbor antiferromagnetic interactions. The moments on Mn atoms align within (111) planes, forming ferromagnetic sheets that stack along the $[111]$ axis such that the magnetization vector reverses between adjacent sheets [1]. The magnetic moments are known to orient themselves parallel to a single direction perpendicular to the $[111]$ stacking axis, but their orientation within the (111) planes is not known [2,3].

From an experimental perspective, the difficulty one faces in determining the orientation of the magnetic moments is that Bragg intensities are sensitive only to the angle the average magnetization vector forms with the stacking axis [4]; moreover, attempts to determine in-plane magnetic anisotropy terms from magnon dispersion curves failed as the measured values were smaller than the experimental accuracy [5]. Alternatively, rather straightforward dipole calculations are capable of predicting that the spin orientations lie within (111) planes, but do not provide any further constraints on the direction [6]. Some further studies showed that a single alignment axis existed, but neither the direction of that axis nor the origin of the anisotropy are known [3].

Here we report the nuclear and magnetic structures of MnO at 10 K, as determined by analysis of total neutron scattering data using the reverse Monte Carlo (RMC) method. We show that the method is capable of arriving at the known ordered structure even when started from random spin configurations; moreover, we have observed that—in addition to the rhombohedral distortion of the nuclear lattice—the Mn and O atoms are displaced very slightly from their previously assigned crystallographic positions, and the Mn magnetic moments possess a small out-of-plane component. Both the atomic and spin displacements are modulated along the $[111]$ stacking direction. As such, they provide a source of anisotropy within the (111) ferromagnetic sheets, and consequently may be responsible for the observed spin alignment via magnetostriction effects. This anisotropy allows the diffraction data some sensitivity to the actual spin alignment direction, which we find to occur along the $\langle 11\bar{2}\rangle$ axes.

Our RMC approach differs from previous crystallographic characterizations of MnO in its simultaneous treatment of both Bragg and diffuse scattering data. This method exploits the rich information concerning local structural correlations that is present within diffuse scattering data, within the average structural framework provided by Bragg diffraction. We have recently developed an implementation of the RMC method in the suite of programs RMCPROFILE [7,8], which differs fundamentally from others in its ability to handle scattering data to large magnitudes Q_{max} of the scattering vector. The details of these differences have been discussed in detail elsewhere [8]. The capacity to refine data that span large regions of reciprocal space is important as the real-space resolution one can hope to extract from RMC configurations is given by $\Delta r \simeq 3.791/Q_{max}$. Using experimental facilities such as the GEM instrument at ISIS [9], it is routinely possible to collect high-quality scattering data to $Q_{max} > 40$ Å^{-1}. For magnetic materials, the magnetic contribution to the scattering data is of course negligible for values of $Q \gtrsim 10$ Å^{-1} (and sometimes significantly less), due to its form-factor dependence. However, the exact nature of

this contribution is refined not simply in terms of the distribution of magnetic moment orientations within the RMC configurations, but also through the positions of the magnetic species themselves. In this way, the accurate refinement of the nuclear structure (which does indeed rely on high-Q data) directly impacts on the quality of the magnetic structure one obtains.

The RMC process then involves refinement of the atomic positions and magnetic moments of a large number of atoms contained within a supercell of the known magnetic unit cell, driven by the ability to fit the experimental scattering data $S(Q)$ and observed Bragg intensities. The nuclear contribution to these quantities can be calculated from the RMC configurations as if no magnetic component were present. The magnetic contribution $S_{\mathrm{mag}}(Q)$ to the scattering factor is calculated from the RMC configurations via two real-space correlation functions $A(r)$ and $B(r)$ [10]:

$$S_{\mathrm{mag}}(Q) = \frac{2}{3} c_{\mathrm{M}} \left[\frac{e^2 \gamma}{2 m_e c^2} g J f(Q) \right]^2 + 4\pi\rho c_{\mathrm{M}} \left[\frac{e^2 \gamma}{2 m_e c^2} f(Q) \right]^2 \times \int r^2 \left\{ A(r) \frac{\sin Qr}{Qr} + B(r) \left[\frac{\sin Qr}{(Qr)^3} - \frac{\cos Qr}{(Qr)^2} \right] \right\} dr,$$

where c_{M} is the concentration of the relevant magnetic species, ρ is the number density of magnetic atoms, e, γ, m_e, and c carry their usual meanings, gJ is the magnetic moment, and $f(Q)$ the magnetic Q-dependent scattering form factor. The magnetic contribution to the Bragg intensities is calculated using a standard approach [11].

We collected total neutron scattering data for a powdered sample of MnO at 10 K on the GEM instrument at ISIS [9] over the range of momentum transfers $0.3 < Q < 50$ Å^{-1}. Both Bragg intensities and $S(Q)$ data were used as input for the RMC procedure. Each starting configuration was a supercell of the known magnetic unit cell, with a volume approximately 1000 times larger than the cell shown in Fig. 1(a). In order that we might simplify our calculations, we used a basis unit cell with orthogonal axes $\mathbf{a}'$, $\mathbf{b}'$, $\mathbf{c}'$ related to those of the face-centered cubic unit cell $\mathbf{a}$, $\mathbf{b}$, $\mathbf{c}$ by the transformation

$$\begin{bmatrix} \mathbf{a}' \\ \mathbf{b}' \\ \mathbf{c}' \end{bmatrix} = \begin{bmatrix} \frac{1}{2} & 0 & -\frac{1}{2} \\ \frac{1}{2} & -1 & \frac{1}{2} \\ 2 & 2 & 2 \end{bmatrix} \begin{bmatrix} \mathbf{a} \\ \mathbf{b} \\ \mathbf{c} \end{bmatrix}.$$

This cell is the smallest orthogonal representation of the low temperature rhombohedral cell.

Individual atoms in the starting configurations were given small random displacements (<0.1 Å) from their crystallographic sites (determined by Rietveld refinement), and the initial orientation of the magnetic moment (of magnitude $5.65\mu_B$ [12]) on each Mn atom was assigned randomly to give a homogenous distribution of moments across the configuration. The refinement procedure reproducibly yielded equilibrium magnetic structures that showed essentially identical antiferromagnetic alignment patterns: they consisted of ferromagnetic sheets parallel to the (111) planes, stacked along [111] with alternating magnetization directions between sheets [13]. In all cases, the spin directions were aligned perpendicular to the [111] stacking axis, although different runs produced different ''preferred'' orientations. We emphasize here that the observed ordering behavior was obtained from starting configurations with entirely random spin orientations. That our results reflect all aspects of the known magnetic structure, as deduced previously in both experimental and theoretical investigations, strongly supports the validity of the approach.

It is easily shown that—like Bragg intensities—the real-space correlation functions $A(r)$ and $B(r)$ are insensitive to the average direction along which the Mn magnetic moments align within (111) planes. This result is essentially a consequence of the threefold rotational axis implicit in rhombohedral lattice symmetry. However, we found in our RMC configurations evidence that this symmetry had been broken. For a given equilibrium RMC configuration, the refined spin orientations were systematically rotated by various angles θ about the [111] stacking axis and the goodness of fit determined—*without further refinement*—at each step. The results obtained [Fig. 2(a)] are perhaps initially counterintuitive and reveal two significant features of the magnetic structure. In the absence of symmetry-breaking modulations of the nuclear lattice, one would expect negligible variation with θ [Fig. 2(b)]; this is clearly not the case. Symmetry-breaking modulations would allow some sensitivity in the correlation functions $A(r)$ and $B(r)$ to the preferred spin alignment axis; however, if they were not coupled with the particular spin alignment axis observed in the original ($\theta = 0$) RMC configuration, then the θ dependency of the goodness of fit would reflect the sixfold symmetry of the (111) sublattice

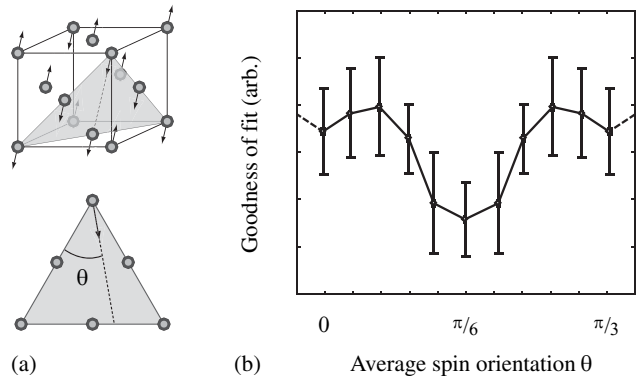

FIG. 1. (a) Representation of the basic antiferromagnetic structure of the Mn sublattice in MnO. The spin orientations (arrows) are known to lie within the (111) ferromagnetic sheets, but their direction θ within these planes is unknown. (b) RMC goodness-of-fit values obtained for equilibrium RMC configurations with differing average spin orientations θ.

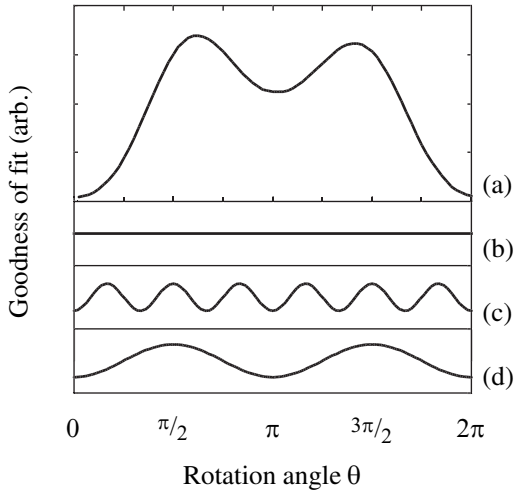

FIG. 2. (a) Observed and (b)–(d) expected RMC goodness-of-fit values for an equilibrium spin configuration rotated to various extents about the [111] axis.

[Fig. 2(c)]. Consequently, we can say that the RMC configurations contain symmetry-breaking lattice modulations that (i) allow the data some sensitivity to the spin alignment axis, and (ii) are coupled to the particular alignment axis arrived at during the RMC refinement procedure. The same qualitative behavior was observed for each of the equilibrium RMC configurations, irrespective of their various spin alignment axes.

A second argument shows that the out-of-plane spin components are also significant in the RMC spin configurations. The various magnetic scattering formalisms—for both $S(Q)$ and Bragg contributions—are symmetric with respect to inversion of the spin orientations. If the out-of-plane spin components were not significant, then rotation of each spin about the [111] axis through an angle of π would be equivalent to the inversion operation. Consequently, one would expect twofold rotational symmetry in the goodness-of-fit plot of Fig. 2(a)—as illustrated in panel (d) of the same figure; the absence of such symmetry signals the relevance of the out-of-plane components to the magnetic structure at 10 K.

To investigate whether the diffraction data revealed any sensitivity to the actual spin alignment axis, we prepared six sets of RMC refinement runs in which the initial spin configurations had been aligned along six different directions in the (111) plane—these were distributed evenly from the $[1\bar{1}0]$ direction ($\theta = 0$) to the $[2\bar{1}\,\bar{1}]$ direction ($\theta = \frac{\pi}{6}$). The initial nuclear configurations used were all identical, and both nuclear and spin configurations had been given small random displacements from their average positions. Each set of runs—corresponding to a single spin alignment axis—contained five configurations in order that some limited statistical weight might be attached to any results obtained. All 30 RMC configurations were refined against the diffraction data, allowing the configurations to accommodate both the correlated nuclear displacements and the out-of-plane spin components known to be present. The observed variation in goodness of fit for differing values of θ [Fig. 1(b)] was found to be almost insignificant in comparison to that associated with the formation of the overall antiferromagnetic structure; nevertheless, the diffraction data show a very slight preference for spin alignment along the $\langle 11\bar{2}\rangle$ axes.

Finally, we sought to establish the nature of the nuclear and magnetic modulations in MnO by collapsing our equilibrium RMC configurations (at $\theta = \frac{\pi}{6}$) onto a single unit cell. The average Mn and O positions were found to vary very slightly from their high-symmetry values, such that all atoms in any given (111) sheets were displaced in the same manner (Mn atoms along a unique axis with no special symmetry; O atoms along the stacking axis), and the overall displacement pattern was periodic along the antiferromagnetic [111] axis [Fig. 3(a)]. These modulations in the nuclear lattice resemble frozen-in phonon modes of the parent high-temperature (cubic) structure at the wave vector $\mathbf{k} = [\frac{1}{6}\,\frac{1}{6}\,\frac{1}{6}]$, and suggest that the magnetic transition at T_N is coupled to the lattice dynamics. Very similar behavior was observed for the out-of-plane spin components [Fig. 3(b)]: the average spin vectors were found to deviate very slightly from the (111) planes with the magnitude of the out-of-plane component also modulated along $\mathbf{k} = [\frac{1}{6}\,\frac{1}{6}\,\frac{1}{6}]$.

While the lattice distortion associated with the paramagnetic-antiferromagnetic transition in MnO is often discussed in terms of a lowering from cubic-to-rhombohedral symmetry, it has been known for some time that the antiferromagnetic structure cannot possess true rhombohedral symmetry [14]. The highest-symmetry space group consistent with a spin alignment axis perpendicular to the "rhombohedral" axis is the monoclinic group $C2/c$. The small observed modulations lower the space group further to $C2$. We were able to refine the modulated structure using the Rietveld refinement program GSAS [15] to give a unit cell with dimensions $a = 5.4458(2)$ Å,

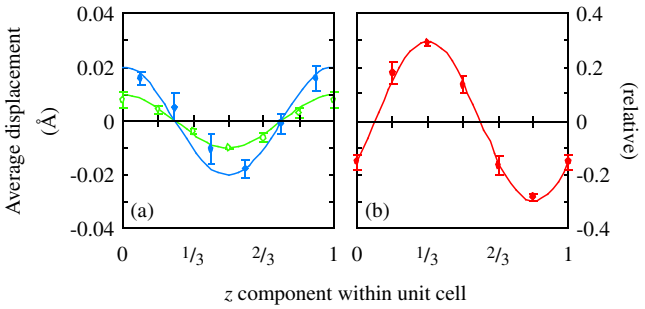

FIG. 3 (color online). (a) Average displacements of the Mn (open circles) and O (solid circles) atoms, and (b) average out-of-plane spin components across the MnO unit cell. The z axis lies parallel to the [111] stacking axis and spans six (111) sheets of Mn atoms.

TABLE I. Atomic positions (round brackets) and spin orientations (square brackets) within the $C2$ MnO unit cell as determined from RMC and GSAS refinements. Relative displacements are $\alpha = -2.072 \times 10^{-3}$, $\beta = 1.011 \times 10^{-2}$, $\gamma = 2.708 \times 10^{-3}$, $\delta = 8.107 \times 10^{-4}$, and $\epsilon = 0.0107$.

Mn1	$(\frac{1}{6}+\alpha, \frac{1}{2}+\beta, \frac{1}{12}+\gamma)$	$[-1, 0, \epsilon]$	O1	$(0, 0, 0)$
Mn2	$(2\alpha, 2\beta, \frac{1}{4}+2\gamma)$	$[1, 0, 2\epsilon]$	O2	$(\frac{1}{3}, 0, \frac{1}{6}+\delta)$
Mn3	$(\frac{1}{3}+\alpha, \beta, \frac{5}{12}+\gamma)$	$[-1, 0, \epsilon]$	O3	$(\frac{1}{6}, \frac{1}{2}, \frac{1}{3}+\delta)$
			O4	$(0, 0, \frac{1}{2})$

$b = 3.14647(13)$ Å, $c = 15.16758(18)$ Å, and $\beta = 89.961(7)°$; the atomic coordinates in this cell are given in Table I and the fit obtained is illustrated in Fig. 4. Interestingly, the monoclinic peak splitting and superlattice Bragg reflections were found to lie within the resolution of the data [Fig. 4]. As such, the GSAS refinement serves primarily to establish an upper limit on the magnitude of the lattice modulations; that RMC refinements can distinguish these features arises from its analysis of the real-space Fourier transforms of the scattering data, in which local symmetry-breaking features are often more apparent. Neither RMC nor GSAS refinements define a length scale along which lattice modulations and spin alignment persist; however, the RMC box size does set a lower bound of approximately 20 Å.

In conclusion, we have shown how RMC analysis of total scattering data has revealed the existence of small modulated variations in the nuclear and magnetic lattices of MnO. These are sufficient to reduce the local lattice symmetry, both providing a mechanism for preferred spin orientation within the (111) planes, and enabling the average alignment direction to be determined from diffraction data. These fine details may be important for *ab initio* calculations, which have typically assumed idealized structures. Having determined the way in which rhombohedral symmetry is broken in this material, this study provides a new paradigm within which to consider a range of otherwise unreconcilable properties of MnO, such as phonon anisotropy [16]. The emphasis in this study on both short-range and long-range structural features has enabled us to make progress where standard magnetic crystallographic tools and simulations have been unable to do so. We have shown the method to be sensitive to coupling between lattice distortions and spin orientations. Thus we believe that total scattering studies may yield new and important information regarding subtle and previously overlooked aspects of the magnetic structures of a wide range of materials.

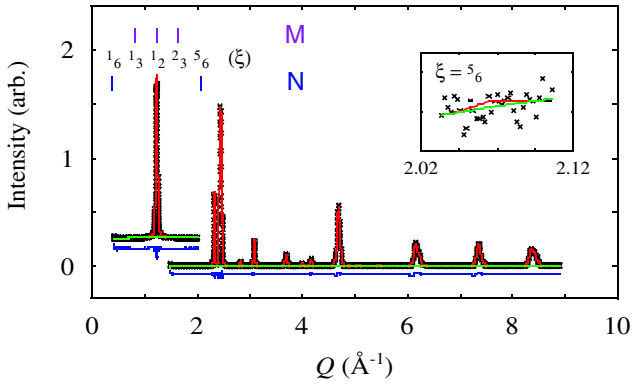

FIG. 4 (color online). Rietveld refinement fit to low-Q scattering data obtained using the program GSAS, incorporating the modulated behavior shown in Fig. 3. The low-Q $(\xi\xi\xi)$ reflections are indicated by "tickmarks," labeled "N" or "M" to indicate nuclear or magnetic character, respectively. The largest isolated superlattice reflection $(\frac{5}{6}\frac{5}{6}\frac{5}{6})$ was found to contain less intensity than the scatter in data (inset).

We acknowledge financial support from EPSRC (U.K.) and from Trinity College, Cambridge, to A. L. G.

*Electronic address: martin@esc.cam.ac.uk

[1] W. L. Roth, Phys. Rev. **110**, 1333 (1958); F. Keffer and W. O'Sullivan, Phys. Rev. **108**, 637 (1957).
[2] H. Shaked, J. Faber, Jr., and R. L. Hitterman, Phys. Rev. B **38**, 11 901 (1988).
[3] R. Bidaux, R. Conte, and J. A. Nasser, J. Appl. Phys. **50**, 1683 (1979); J. Phys. (Paris) **41**, 1317 (1980).
[4] G. Shirane, Acta Crystallogr. **12**, 282 (1959).
[5] G. Pepy, J. Phys. Chem. Solids **35**, 433 (1974).
[6] J. I. Kaplan, J. Chem. Phys. **22**, 1709 (1954).
[7] M. G. Tucker, M. T. Dove, and D. A. Keen, J. Appl. Crystallogr. **34**, 630 (2001).
[8] M. T. Dove, M. G. Tucker, and D. A. Keen, Eur. J. Mineral. **14**, 331 (2002).
[9] A. C. Hannon, Nucl. Instrum. Methods Phys. Res., Sect. A **551**, 88 (2005).
[10] I. A. Blech and B. L. Averbach, Physics (Long Island City, N.Y.) **1**, 31 (1964); D. A. Keen and R. L. McGreevy, J. Phys. Condens. Matter **3**, 7383 (1991).
[11] M. T. Dove, Eur. J. Mineral. **14**, 203 (2002).
[12] A. Mellergård *et al.*, J. Phys. Condens. Matter **10**, 9401 (1998).
[13] The crystallographical nomenclature refers to the parent cubic structure of the paramagnetic phase, and assumes that the unique rhombohedral axis lies along [111].
[14] A. K. Cheetham and D. A. O. Hope, Phys. Rev. B **27**, 6964 (1983).
[15] A. C. Larson and R. B. Von Dreele, General Structural Analysis System (GSAS), Los Alamos National Laboratory Report No. LAUR 86-748, 2000; B. H. Toby, J. Appl. Crystallogr. **34**, 210 (2001).
[16] S. Massidda *et al.*, Phys. Rev. Lett. **82**, 430 (1999); E. M. L. Chung *et al.*, Phys. Rev. B **68**, 140406(R) (2003).